

# Surface-Focused Seismic Holography of Sunspots: I. Observations

D.C. Braun · A.C. Birch

Received: 5 October 2007 / Accepted: 14 February 2008 / Published online: 7 March 2008  
© Springer Science+Business Media B.V. 2008

**Abstract** We present a comprehensive set of observations of the interaction of  $p$ -mode oscillations with sunspots using surface-focused seismic holography. Maps of travel-time shifts, relative to quiet-Sun travel times, are shown for incoming and outgoing  $p$  modes as well as their mean and difference. We compare results using phase-speed filters with results obtained with filters that isolate single  $p$ -mode ridges, and we further divide the data into multiple temporal frequency bandpasses. The  $f$  mode is removed from the data. The variations of the resulting travel-time shifts with magnetic-field strength and with the filter parameters are explored. We find that spatial averages of these shifts within sunspot umbrae, penumbrae, and surrounding plage often show strong frequency variations at fixed phase speed. In addition, we find that positive values of the mean and difference travel-time shifts appear exclusively in waves observed with phase-speed filters that are dominated by power in the low-frequency wing of the  $p_1$  ridge. We assess the ratio of incoming to outgoing  $p$ -mode power using the ridge filters and compare surface-focused holography measurements with the results of earlier published  $p$ -mode scattering measurements using Fourier – Hankel decomposition.

**Keywords** Active regions · Magnetic fields · Helioseismology · Observations

## 1. Introduction

The use of solar acoustic ( $p$ -mode) waves to probe the subsurface structure of active regions (ARs) was first proposed by Thomas, Cram, and Nye (1982). Although efforts have been made to deduce properties of sunspots from interpretations of oscillations observed within

---

Helioseismology, Asteroseismology, and MHD Connections  
Guest Editors: Laurent Gizon and Paul Cally

D.C. Braun (✉) · A.C. Birch  
NWRA, CoRA Division, Boulder, CO, USA  
e-mail: [dbraun@cora.nwra.com](mailto:dbraun@cora.nwra.com)

A.C. Birch  
e-mail: [aaronb@cora.nwra.com](mailto:aaronb@cora.nwra.com)

sunspots (see reviews by Lites, 1992, and Bogdan, 2000), recent advances in sunspot seismology have been largely driven by the observations of the strong influences of sunspots (and ARs in general) on externally impinging  $p$  modes. This includes both absorption (*e.g.*, Braun, Duvall, and LaBonte, 1988; Bogdan *et al.*, 1993) and changes in phase (often characterized in terms of a change in travel time; *e.g.*, Braun *et al.*, 1992; Braun, 1995; Duvall *et al.*, 1996). A prevalent, largely phenomenological, approach to exploiting the travel-time shifts (relative to travel times in the quiet Sun) to model the subsurface properties of sunspots has been the characterization of the spot as a perturbation in the background sound speed. These types of models have been constructed by using observations from a variety of local-helioseismic techniques, including Fourier–Hankel decomposition (*e.g.*, Fan, Braun, and Chou, 1995), time–distance analysis (*e.g.*, Kosovichev, 1996; Kosovichev, Duvall, and Scherrer, 2000; Jensen *et al.*, 2001), ring diagrams (*e.g.*, Basu, Antia, and Bogart, 2004), and holography (*e.g.*, Lindsey and Braun, 2005b). The discovery of travel-time asymmetries between waves propagating toward and away from sunspots (Duvall *et al.*, 1996) have led to the inclusion of subsurface flows in many of these efforts. Travel times inferred from time–distance (TD) helioseismology have in particular been inverted to model flows and sound-speed perturbations by using a variety of assumptions including Fermat’s principle and the ray approximation (*e.g.*, Kosovichev and Duvall, 1997; Kosovichev, Duvall, and Scherrer, 2000; Zhao, Kosovichev, and Duvall, 2001; Hughes, Rajaguru, and Thompson, 2005), the Fresnel-zone approximation (*e.g.*, Jensen *et al.*, 2001; Couvidat *et al.*, 2004), and the Born approximation (Couvidat, Birch, and Kosovichev, 2006). A consensus of many of these 3D inversions has emerged consisting of a relatively shallow (approximately 3 Mm deep) “slower” sound-speed perturbation above a “faster” sound-speed layer extending 10 Mm or more below the photosphere (see the review by Gizon and Birch, 2005).

These phenomenological models have been useful as foundations for developing both forward and inverse methods under a variety of approximations and assumptions (Gizon and Birch, 2005). At the same time, uncertainties about the degree to which the magnetic fields may contribute (in ways other than through associated thermal perturbations and flows) to phase or travel-time shifts, particularly in the near-surface layers, have persisted. Most local-helioseismic models of travel-time shifts, to date, do not include provisions for contributions from unresolved near-surface layers. [Near the photosphere, the typical vertical resolution provided by observed  $p$  modes is around 1 Mm (*e.g.*, Couvidat, Birch, and Kosovichev, 2006).] Notable exceptions include some 1D (horizontally invariant) structural inversions obtained from ring-diagram analyses (*e.g.*, Simmons and Basu, 2003; Basu, Antia, and Bogart, 2004).

Some observations and inferred sound-speed models may show direct evidence of strong near-surface contributions to the helioseismic signatures associated with ARs. An early example of this is the predominantly near-surface sound-speed perturbation consistent with Fourier–Hankel analysis (Fan, Braun, and Chou, 1995). Birch, Braun, and Hanasoge (2008; Paper 2) examine the relevance of this particular result to a more recent modeling effort. Lindsey and Braun (2005b) have shown that helioseismic signatures beneath ARs obtained by using holography largely vanish when a surface (“showerglass”) phase shift, empirically related to photospheric magnetic flux density, is removed from the data. Some peculiar properties of the 3D time–distance inversions have also been presented as evidence for surface “contamination.” Korzennik (2006) demonstrated that an inferred subsurface sound-speed “plume” structure depends critically on the inclusion of observations made within a sunspot penumbra and umbra. A test of inversions for flows performed by masking only the umbra showed little effect of the mask (Zhao and Kosovichev, 2003). Ringlike regions of enhanced sound speed in TD inversions of sunspots have also been examined as possible artifacts

arising from the surface (Couvidat and Rajaguru, 2007). Surface effects in magnetic fields also include changes in the upper turning points (*e.g.*, Kosovichev and Duvall, 1997; Braun and Lindsey, 2000; Barnes and Cally, 2001). The observed reduction of *p*-mode amplitudes in spots has been shown to contribute to travel-time shifts independent of actual structural changes (Rajaguru *et al.*, 2006) as has reduced wave excitation (Hanasoge *et al.*, 2007; Parchevsky, Zhao, and Kosovichev, 2008).

Schunker *et al.* (2005) and Schunker, Braun, and Cally (2007) found that travel-time shifts obtained from seismic holography in sunspot penumbrae vary with the line-of-sight angle projected onto the plane containing the magnetic field and the vertical direction. A similar effect has also been noted by Zhao and Kosovichev (2006) with time–distance measurements. A satisfactory theory explaining these observations remains to be constructed, but some preliminary suggestions include mode conversion (Schunker and Cally, 2006) or radiative transfer effects in combination with mode propagation asymmetries (Rajaguru *et al.*, 2007). Whatever the cause, the observed line-of-sight dependence of travel-time shifts implies that a significant component of the shifts, at least in sunspot penumbrae, must be photospheric in origin.

In 1D inversions in global helioseismology (*e.g.*, Christensen-Dalsgaard, Gough, and Perez Hernandez, 1988) and ring-diagram analyses (*e.g.*, Basu, Antia, and Bogart, 2004), surface effects are largely characterized by their frequency-dependent contribution to the helioseismic signatures (mode or ridge frequencies). In contrast, the observations used in 3D travel-time inversions are typically made over a single wide-frequency bandpass and do not easily allow the assessment of possible frequency-dependent surface terms. However, there is increasing evidence for frequency variations in the travel-time shifts observed in ARs (Braun and Lindsey, 2000; Chou, 2000; Lindsey and Braun, 2004b; Braun and Birch, 2006; Couvidat and Rajaguru, 2007). Braun and Birch (2006) found evidence for a frequency variation, at fixed phase speed, of the travel times measured in active regions using helioseismic holography. This variation exceeds the smaller frequency variation expected from travel-time shifts computed from a proxy sound-speed model, with properties similar to recent two-component 3D inversions, by using the ray approximation.

The observed travel-time asymmetries in sunspots (differences in travel times between the incoming and outgoing propagating waves) have been interpreted and modeled as due to flows (Duvall *et al.*, 1996; Zhao, Kosovichev, and Duvall, 2001; Zhao and Kosovichev, 2003). The shallow inflows, within the first 3 Mm below the surface, characteristic of some of these *p*-mode-based TD models appear to be inconsistent with outflows inferred from other methods including *f*-mode time–distance analysis (Gizon, Duvall, and Larsen, 2000) and holography (Braun, Birch, and Lindsey, 2004). Some questions have been raised whether travel-time asymmetries may arise from other mechanisms, including the suppression of acoustic sources (Gizon and Birch, 2002; Hanasoge *et al.*, 2007) or absorption (Woodard, 1997; Lindsey, Schunker, and Cally, 2007).

Including magnetic fields in helioseismic models of sunspots appears to be a substantially more formidable task than constructing models that include only thermal perturbations. Some progress has been made with MHD models of the absorption in sunspots observed from Fourier–Hankel decomposition (*e.g.*, see the review by Bogdan and Braun, 1995). More recent efforts have also addressed the observed phase shifts (*e.g.*, Cally, Crouch, and Braun, 2003; Crouch *et al.*, 2005; Gordovskyy and Jain, 2007). It is expected that considerable advances in modeling helioseismic data will follow from the current development and application of hydrodynamic (HD) and magnetohydrodynamic (MHD) simulations (*e.g.*, Jensen, Duvall, and Jacobsen, 2003; Tong *et al.*, 2003; Mansour *et al.*, 2004; Werne, Birch, and Julien, 2004; Benson, Stein, and Nordlund, 2006; Hanasoge and Duvall, 2007; Hanasoge, Duvall, and Couvidat, 2007; Khomenko and Collados, 2006; Shelyag, Erdélyi, and

Thompson, 2006, 2007; Cameron, Gizon, and Daifallah, 2007; Cameron, Gizon, and Duvall, 2008).

Our primary motivation in this paper is to expand the measurements of Braun and Birch (2006). We hope that a comprehensive exposition of helioseismic observations of travel-time shifts, and their dependence on  $p$ -mode properties, will promote and support improved modeling efforts, including the use of numerical simulations. As we are specifically interested in the importance of near-surface effects we also examine the relationship between the observed travel-time shifts and the photospheric magnetic field. Of particular importance is the measurement of frequency variations of the travel-time shifts, by using methods similar to Braun and Birch (2006). However, we extend those measurements to include both mean travel-time shifts and travel-time asymmetries, and we determine spatial averages of these quantities over sunspot umbrae, penumbrae, and other magnetic regions. Our principal tool is surface-focused helioseismic holography (e.g., Braun and Lindsey, 2000; Braun and Birch, 2006), for which the travel-time shifts are expected to have the most sensitivity to near-surface perturbations. The use of surface-focus holography (described in Section 2) contrasts this work with other recent (“lateral-vantage”) holographic studies of ARs (e.g., Lindsey and Braun, 2005a, 2005b). In addition, to ensure a meaningful comparison of our results (described in Section 3) to TD observations we use narrow annular pupils and corresponding phase-speed filters as discussed in Section 3.1. An overriding theme in our findings is a strong sensitivity of the results to the choice of filter and frequency bandwidth employed. To investigate this further, we also employ filters centered on the  $p$ -mode ridges (Section 3.2). The ridge-based filters allow a detailed comparison of surface-focused holography measurements of both travel-time shifts and absorption with published results of Fourier–Hankel analysis (Section 3.3).

## 2. Analysis

Helioseismic holography (HH) is a method based on the phase-coherent imaging of the solar interior acoustic field. In HH one computationally extrapolates the surface acoustic field into the solar interior (Lindsey and Braun, 1997, 2000) to estimate the amplitudes of the waves propagating into and out of a focus point at a chosen depth and position in the solar interior. These amplitudes, called the ingression ( $H_-$ ) and egression ( $H_+$ ) are estimated by a convolution of the surface oscillation signal ( $\psi$ ) (typically the line-of-sight component of velocity observed from Dopplergrams) with appropriate Green’s functions (Lindsey and Braun, 2000). For this work, the Green’s functions are computed in the eikonal formulation (Lindsey and Braun, 1997, 2000). For surface-focused HH, the Green’s functions represent propagators that evolve the acoustic field forward or backward in time from a position on the solar surface into the solar interior, and back up to the surface focus. To select a particular set of  $p$  modes, these functions are evaluated over a chosen annular pupil. A dispersion correction, empirically determined from statistics obtained from measurements in the quiet Sun, is applied to the computation of the Green’s functions (see Lindsey and Braun, 2000).

The basis of our analysis consists of what are termed *local control correlations* (Lindsey and Braun, 2004a, 2005a). These are directly comparable to center-annulus TD correlations (e.g., Duvall *et al.*, 1996; Braun, 1997). In the space-frequency domain, the correlation

$$C_+(\mathbf{r}) = \langle H_+(\mathbf{r}, \nu) \psi^*(\mathbf{r}, \nu) \rangle_{\Delta\nu} \quad (1)$$

describes the egression control correlation, and

$$C_-(\mathbf{r}) = \langle \psi(\mathbf{r}, \nu) H_-^*(\mathbf{r}, \nu) \rangle_{\Delta\nu} \quad (2)$$

describes the ingression control correlation. Here,  $\psi(\mathbf{r}, \nu)$  represents the temporal Fourier transform of the surface wave field,  $\nu$  is the temporal frequency,  $\mathbf{r}$  is the horizontal position on the solar surface, and  $H_-(\mathbf{r}, \nu)$  and  $H_+(\mathbf{r}, \nu)$  represent the temporal Fourier transforms of the ingression and egression, respectively. The asterisk denotes complex conjugation, and the angle brackets indicate an average over a chosen positive frequency range  $\Delta\nu$ .

The primary quantities of interest are the travel-time shifts, which are related to the phase of the correlations,

$$\delta\tau_{\pm} = \arg[C_{\pm}(\mathbf{r})]/2\pi\nu_0, \quad (3)$$

where  $\nu_0$  is the central frequency of the bandpass  $\Delta\nu$ . These represent travel-time shifts of the observed incoming ( $\tau_-$ ) or outgoing ( $\tau_+$ ) waves, as sampled by a chosen filter, relative to the travel times expected for the same ensemble of waves propagating in the solar model used to compute the Green's functions. Small systematic deviations of the quiet-Sun values from zero, which vary with pupil size and filter and are likely caused by imperfections in the Green's functions and dispersion correction, are removed by subtracting averaged quiet-Sun values from the observed control correlation phases. Of interest are the mean travel-time shift,  $\delta\tau_{\text{mean}} = (\delta\tau_+ + \delta\tau_-)/2$ , and the difference (or travel-time asymmetry),  $\delta\tau_{\text{diff}} = \delta\tau_+ - \delta\tau_-$ .

A 27-hour sequence of full-disk Dopplergrams with one-minute cadence, obtained from the Michelson Doppler Imager (MDI; Scherrer *et al.*, 1995) onboard the *Solar and Heliospheric Observatory* (SOHO), was used in this study. The data set starts on 1 April 2002, 21:01 UT, and includes several sunspot groups (NOAA groups 9885, 9886, 9887, and 9888) within a  $60^\circ \times 60^\circ$  Postel-projected region. This area was tracked at the Carrington rotation rate and includes four sunspots with penumbral radii greater than 15 Mm as well as other smaller spots. The three largest sunspots are very similar in size, with mean umbral and penumbral radii of 7 and 18 Mm, respectively.

The following steps summarize the general data reduction: (1) projection of the desired region from full-disk Dopplergrams to a Postel projection that rotates with a fixed Carrington rate, (2) temporal detrending by subtraction of a linear fit to each pixel signal in time, (3) removal of poor quality images, identified by a five- $\sigma$  deviation of any pixel from the linear trend, (4) Fourier transform of the data in time, (5) (optional) correction for the amplitude suppression in magnetic regions (Rajaguru *et al.*, 2006), (6) spatial Fourier transform of the data and multiplication by a chosen filter, (7) extraction of the desired frequency bandpass, (8) computation of Green's functions over the appropriate pupil, (9) computation of ingression and egression amplitudes by a 3D convolution of the data with the Green's functions, and (10) computation of the travel-time shift maps by Equations (1)–(3).

The optional correction for amplitude suppression (step 5) involves dividing the amplitude of each pixel in the data by its root-mean-square value over the frequency bandpass. In step 6 we have used two sets of filters: phase-speed filters and ridge filters. Their description and the results obtained from each set are described in Section 3.1 and Section 3.2. For the phase-speed filters (Section 3.1) we compare results with and without the amplitude-suppression correction. The difference is relatively small and, for the ridge-filtering (Section 3.2), we use only uncorrected data.

### 3. Observations

#### 3.1. Phase-Speed Filters

The phase-speed filters used are of the type specified by Couvidat, Birch, and Kosovichev (2006); namely, the three-dimensional Fourier transform of the data (step 6) is multiplied by

a function

$$F(\mathbf{k}, \nu) = \exp[-(2\pi\nu/|\mathbf{k}| - w)^2/2\delta w^2], \quad (4)$$

where  $w$  and  $\delta w$  are the mean phase speed and filter width, respectively. We use the same set of ten filters (denoted A through J) of Braun and Birch (2006) with parameters listed in Table 1 of that paper. These filters are of the same type, but are somewhat narrower in width, than the eleven common filters often employed in TD analyses (e.g., Couvidat, Birch, and Kosovichev, 2006; Zhao and Kosovichev, 2006). Each filter is used with a corresponding pupil, over which the ingress and egress are evaluated. This pupil is a complete annulus defined so that acoustic rays at a frequency of  $\nu = 3.5$  mHz reaching the inner and outer radii span the full width at half maximum (FWHM) of the squared filter. The parameter  $\delta w$  is related to the FWHM by  $\delta w = \text{FWHM}/[2(\ln 2)^{1/2}]$ . The filters were chosen such that the sets of FWHM and corresponding pupils span a continuous range of phase speed and radius, respectively.

All of the phase-speed filters used also remove the contribution of the  $f$  mode, a practice first used by Giles (2000). Our  $f$ -mode cutoff consists of a high-pass filter with Gaussian roll-off in temporal frequency. The position and rate of the roll-off varies with spatial wavenumber such that full transmission occurs at a frequency midway between the  $f$  mode and  $p_1$  ridges and  $10^{-7}$  transmission occurs at the frequency of the  $f$  mode.

The filters are applied to, and the travel-time shift maps computed from, portions of the data extracted in 1-mHz-wide frequency bandpasses centered at 2, 3, 4, and 5 mHz. We also compute travel-time shifts over a wider bandpass (2.5–5.5 mHz) typical of common TD measurements. The use of narrow frequency bandpasses, although frequently employed in HH, differs from typical applications of TD correlations. Consequently, the wide bandpass measurements provide a useful check and basis for comparison. It should be noted, however, that the power spectra of solar acoustic oscillations are naturally limited in bandwidth. Power spectra computed by using typical phase-speed filters applied to MDI data, without any additional temporal filtering, show a concentration of between 60% and 90% of the power within a 1-mHz bandwidth, depending on the choice of phase-speed filter.

Some maps of travel-time shifts computed with phase-speed filters are shown in Figures 1 and 2. Figure 1 shows maps of  $\delta\tau_-$  (top panels) and  $\delta\tau_+$  (bottom panels); Figure 2 shows the corresponding maps of  $\delta\tau_{\text{mean}}$  (top) and  $\delta\tau_{\text{diff}}$  (bottom). The maps are stacked into columns of increasing phase speed (left to right) and rows representing increasing frequency (bottom to top). For simplicity we will refer to each map by a number–letter combination denoting filter and frequency combination; for example, “4B” refers to filter B applied to the frequency bandpass centered at 4 mHz. Because of the filter masking the  $f$  mode, and the decrease in acoustic wave amplitudes at frequencies below the  $p_1$  ridge, only a subset of possible frequency–filter combinations produce meaningful correlations. The maps analyzed here are limited to filters 2D–2J, 3B–3J, 4A–4J, and 5A–5J.

Individual maps exhibit spatial relationships between the travel-time shifts and the surface magnetic flux explored below. The stacking of maps in Figures 1 and 2 reveals several striking properties of the travel-time shifts, including frequency dependencies of  $\delta\tau_+$ ,  $\delta\tau_-$ ,  $\delta\tau_{\text{mean}}$ , and  $\delta\tau_{\text{diff}}$  at all phase-speed filters, and a surprising connection between the sign of the shifts and the value of the central frequency of the filter with respect to the frequency of the  $p_1$  ridge. In particular, positive travel-time shifts (for both incoming and outgoing waves) are observed exclusively in frequency bandwidths that are centered below the  $p_1$  ridge, shown by the solid line in Figures 1 and 2. Maps of  $\delta\tau_+$ ,  $\delta\tau_-$ ,  $\delta\tau_{\text{mean}}$ , and  $\delta\tau_{\text{diff}}$  for filters with frequencies closest to the  $p_1$  ridge (i.e., 4B, 3C, and 2D—not shown) show positive

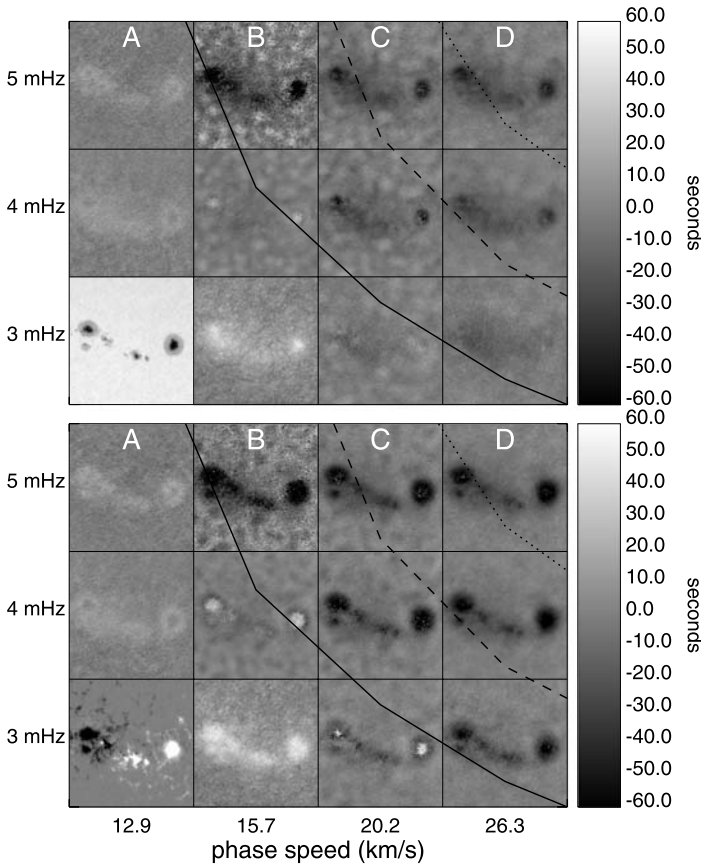


**Figure 1** Maps of travel-time shifts  $\delta\tau_-$  (top panels) and  $\delta\tau_+$  (bottom panels) covering a portion of the region studied and showing sunspot group 9885. The columns of maps labeled A through D indicate the phase-speed filter used; the rows indicate the frequency bandpass. The solid jagged line running diagonally through the panels connects the location of the  $p_1$  ridge in the  $v-w$  domain for each filter, with the centers of the maps assigned to values of frequency and phase speed as indicated on the left and bottom edges of the plot. The dashed and dotted lines indicate the locations of the  $p_2$  and  $p_3$  ridges, respectively. The map in the lowest left position of the top set of panels shows an MDI continuum intensity image; the map in the same position in the bottom set shows a line-of-sight magnetogram.

shifts near sunspot umbra and negative travel-time shifts elsewhere in the ARs. At frequencies above (below) these values, the filters yield exclusively negative (positive) travel-time shifts. Filters E–J (not shown) exhibit trends similar to filter D. For these filters, negative values for  $\delta\tau_+$  and  $\delta\tau_-$  are observed throughout the active region. Both incoming and outgoing time shifts measured with the larger phase-speed filters increase with increasing frequency, with the values of the outgoing shifts exceeding the incoming shifts. These filters (E–J) show AR travel-time differences ( $\delta\tau_{diff}$ ) that decrease with increasing frequency.

As noted earlier by Braun and Birch (2006), the travel times are nonlinearly related to the surface magnetic-flux density. The quantity  $B_{tot}$  is derived from an MDI line-of-sight magnetogram by assuming the magnetic field is the gradient of a potential and is used as a proxy for the total flux density. Figures 3 and 4 show plots of travel-time shifts against  $B_{tot}$  for phase-speed filters B and E, respectively. For clarity, the scatter of individual pixel

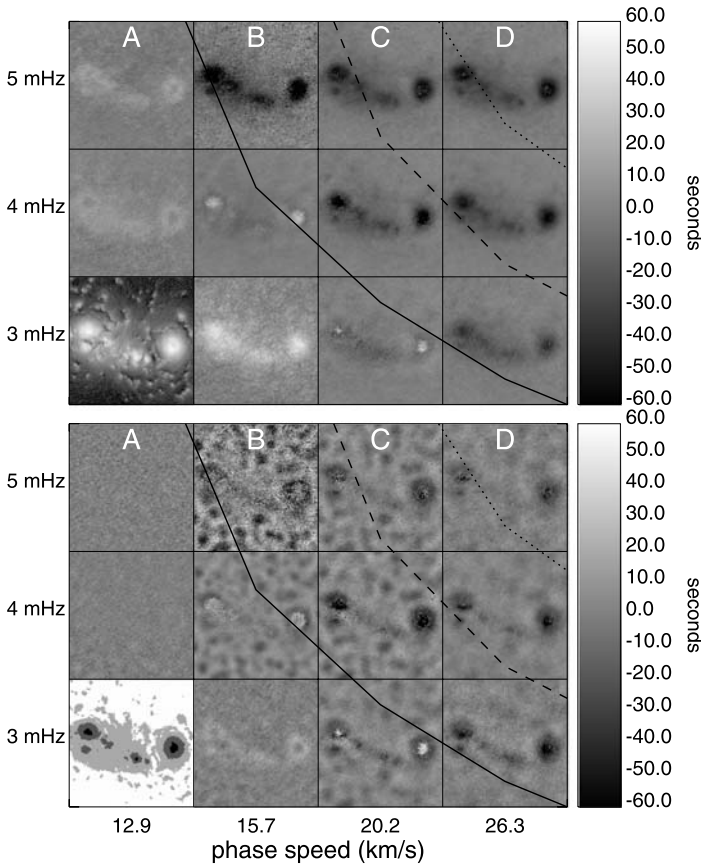


**Figure 2** Maps of the travel-time shifts  $\delta\tau_{\text{mean}}$  (top panels) and  $\delta\tau_{\text{diff}}$  (bottom panels) covering a portion of the region studied and showing sunspot group 9885. The columns of maps labeled A through D indicate the phase-speed filter used; the rows indicate the frequency bandpass. The solid jagged line running diagonally through the panels connects the location of the  $p_1$  ridge in the  $v-w$  domain for each filter, with the centers of the maps assigned to values of frequency and phase speed as indicated on the left and bottom edges of the plot. The dashed and dotted lines indicate the locations of the  $p_2$  and  $p_3$  ridges, respectively. The map in the lowest left position of the top set of panels shows  $B_{\text{tot}}$  (see text); the image in the same position in the bottom set isolates in shades of gray different portions of the AR for study (see text).

values is not shown (although see Figure 1 of Braun and Birch, 2006, for some examples). Instead, Figures 3 and 4 show the average of the shifts derived from bins equally spaced in the logarithm of the flux density. Solid (dotted) lines indicate time shifts computed with (without) the amplitude-suppression correction discussed in Section 2. The effect of the correction is to decrease the travel-time shifts, especially at lower phase speeds (and smaller pupils) and in regions of high flux densities typical of the sunspot umbrae and penumbrae, by amounts on the order of one to ten seconds. Vertical bars in Figures 3 and 4, and in most of the other plots shown in this paper, indicate the total deviation (maxima minus minima) of the averaged value as determined within three independent subregions containing the three largest sunspots. Thus, the bars include contributions not only from sources of random error but also from potentially systematic differences between sunspots. Typically, however, these deviations as a whole are very small.

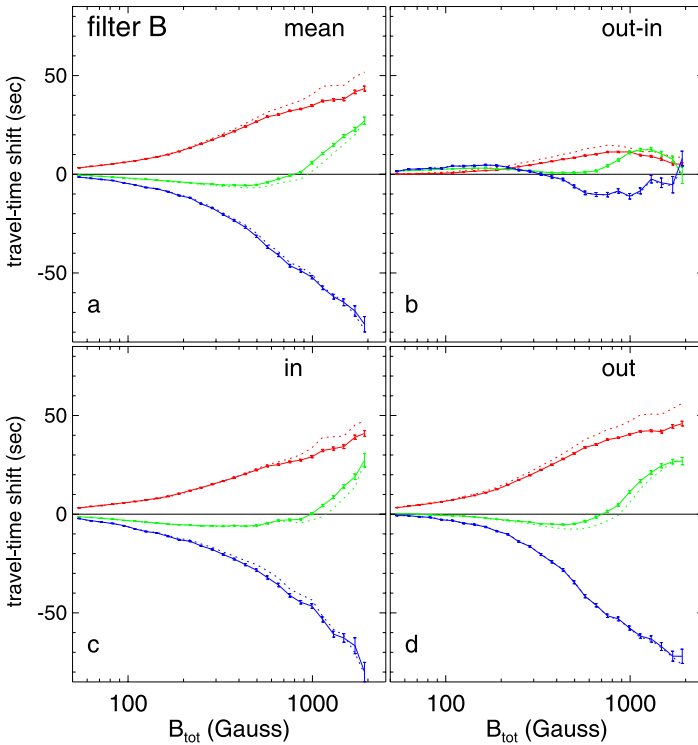


**Figure 3** Travel-time shifts for filter B: (a) the mean travel-time shift, (b) the travel-time difference, (c) the incoming travel-time shift, and (d) the outgoing travel-time shift as functions of the magnetic field  $B_{tot}$ . Solid (dotted) lines connect averaged travel-time shifts, averaged over equally spaced bins in the logarithm of the flux density, computed with (without) an amplitude-suppression correction (see text). Red, green, and blue lines indicate frequencies of 3, 4, and 5 mHz, respectively. Vertical bars indicate the total deviation (maxima minus minima) of the averages of three independent subregions containing the three largest sunspots.

The frequency variation shown for filter B (Figure 3) is typical of the results with smaller phase speeds (and smaller pupils) that undergo the transition from positive time shifts (at sub- $p_1$  frequencies) to negative time shifts (at frequencies higher than the  $p_1$  ridge). The different frequencies shown in Figure 3a exhibit the three types of dependence on flux density of the mean travel-time shift described by Braun and Birch (2006). The travel-time differences (Figure 3b) show similar trends except at the highest flux densities, where the results for all frequencies approach zero. For filter E (Figure 4), it is observed that the frequency variations are in general larger for  $\delta\tau_-$  shifts than for  $\delta\tau_+$ . As noted earlier, the differences  $\delta\tau_{diff}$  for these larger phase speeds show larger shifts at lower frequencies. This trend is opposite to that observed with the mean shifts  $\delta\tau_{mean}$ .

As Braun and Birch (2006) note, the close relationship between  $\delta\tau_{mean}$  and  $B_{tot}$  is consistent with predominately near-surface perturbations, but it does not rule out subsurface perturbations that may very well correlate with surface flux. As discussed in Section 1, the variation of travel-time shifts with both temporal frequency and phase speed is of critical importance in understanding the depth variations of the underlying perturbations. In particular, Braun and Birch (2006) have suggested that the variation with frequency, at fixed phase speeds, of travel-time shifts may be a signature of surface effects (see also Paper 2).

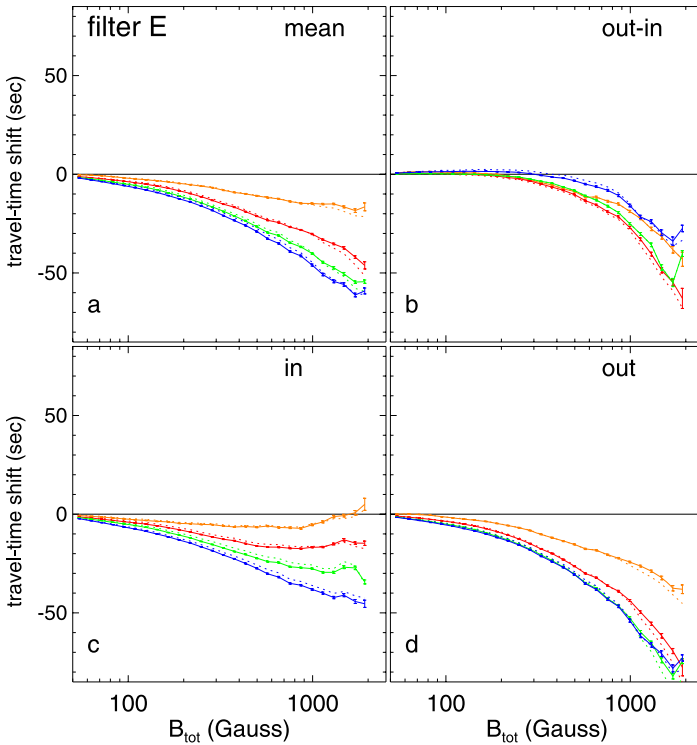


**Figure 4** Travel-time shifts for filter E: (a) the mean travel-time shift, (b) the travel-time difference, (c) the incoming travel-time shift, and (d) the outgoing travel-time shift as functions of the magnetic field  $B_{\text{tot}}$ . Solid (dotted) lines connect averaged travel-time shifts, averaged over equally spaced bins in the logarithm of the flux density, computed with (without) an amplitude-suppression correction (see text). Orange, red, green, and blue lines indicate frequencies of 2, 3, 4, and 5 mHz, respectively. Vertical bars indicate the total deviation (maxima minus minima) of the averages of three independent subregions containing the three largest sunspots.

To quantify these variations, we compute spatial averages of the travel-time shifts over three types of regions characteristic of the sunspot groups. The first two types are sunspot umbrae and penumbrae, identified by brightness values of less than 50% and 92% of the mean MDI continuum values, respectively. The third region of interest (which we simply call “plage”) is identified by values of  $B_{\text{tot}}$  above 100 gauss and excluding areas previously marked as umbrae or penumbrae. The panel in the lowest left corner of Figure 2 illustrates in increasingly darker shades of gray the three regions (plage, penumbrae, and umbrae) identified in this manner around NOAA 9885. The umbral and penumbral averages are of particular importance since they represent time shifts experienced by waves propagating through the immediate subsurface layers of a sunspot (*e.g.*, within 10 Mm depth below a 30-Mm-diameter spot). Figures 5, 6, and 7 show the spatially averaged time shifts for the umbrae, penumbrae, and plage, respectively. These figures quantify many of the properties already noted in the travel-time shift maps, including the strong frequency variations at each fixed phase speed and the changes of sign at smaller phase speeds. Figures 5–7 also include the measurements made with the wide temporal bandpass (2.5–3.5 mHz). These values, as expected from the relative contributions of modes in the power spectra, fall largely between the results obtained in the 3- and 4-mHz bandpasses. Also noteworthy is that, for the plage,

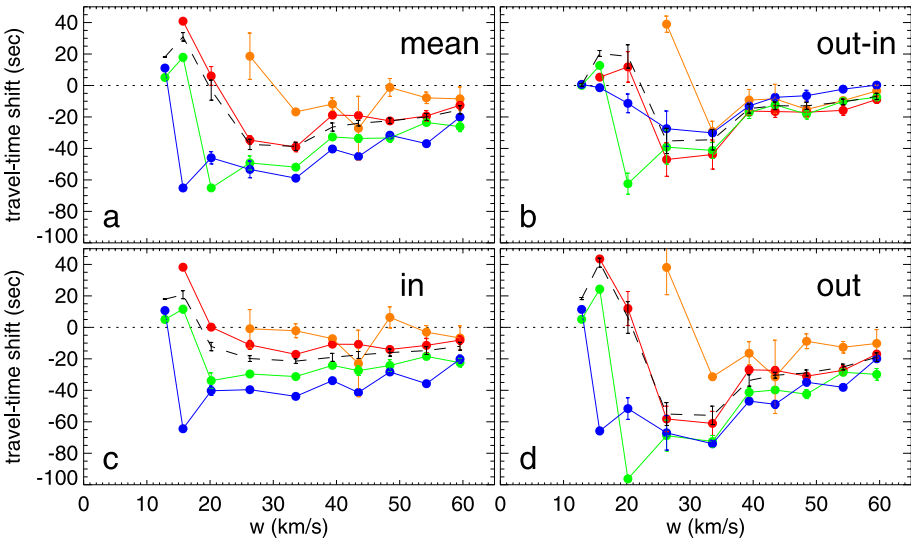


**Figure 5** (a) The mean travel-time shift, (b) the travel-time difference, (c) the incoming travel-time shift, and (d) the outgoing travel-time shift, averaged over the sunspot umbrae, as functions of the phase speed  $w$ . Yellow, red, green, and blue lines indicate frequencies of 2, 3, 4, and 5 mHz, respectively. The black dashed line indicates the use of the wide (2.5–5.5 mHz) frequency bandpass. Vertical bars indicate the total deviation (maxima minus minima) of the averages of three independent subregions containing the three largest sunspots.

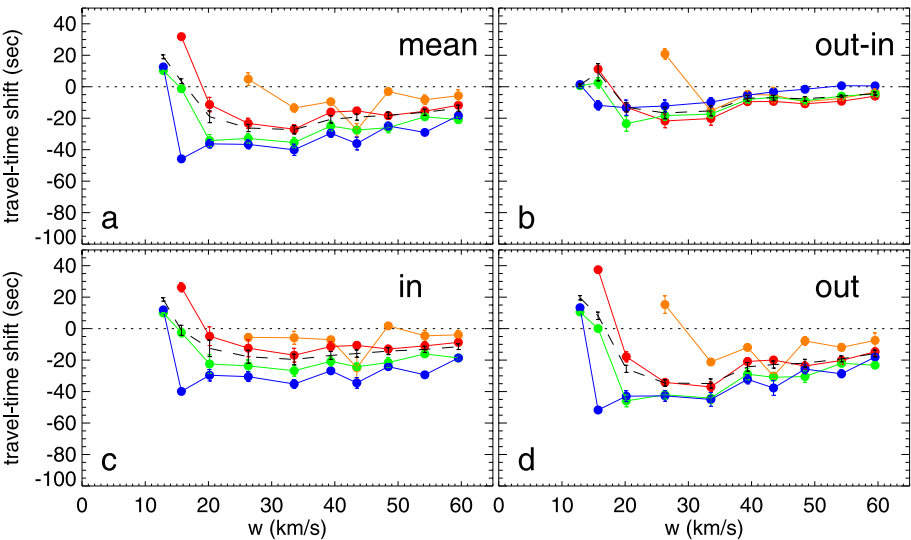


**Figure 6** (a) The mean travel-time shift, (b) the travel-time difference, (c) the incoming travel-time shift, and (d) the outgoing travel-time shift, averaged over the sunspot penumbrae, as functions of the phase speed  $w$ . Yellow, red, green, and blue lines indicate frequencies of 2, 3, 4, and 5 mHz, respectively. The black dashed line indicates the use of the wide (2.5–5.5 mHz) frequency bandpass. Vertical bars indicate the total deviation (maxima minus minima) of the averages of three independent subregions containing the three largest sunspots.

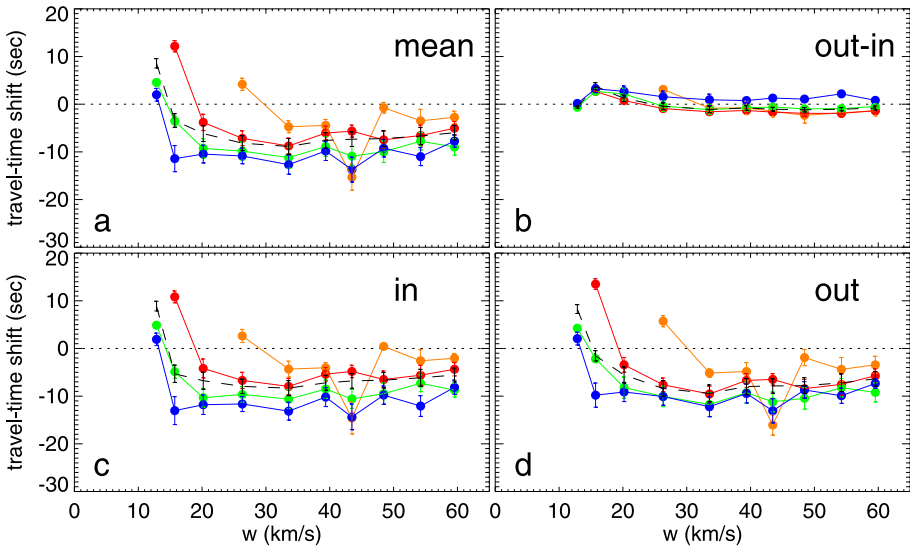


**Figure 7** (a) The mean travel-time shift, (b) the travel-time difference, (c) the incoming travel-time shift, and (d) the outgoing travel-time shift, averaged over the plage, as functions of the phase speed  $w$ . Yellow, red, green, and blue lines indicate frequencies of 2, 3, 4, and 5 mHz, respectively. The black dashed line indicates the use of the wide (2.5–5.5 mHz) frequency bandpass. Vertical bars indicate the total deviation (maxima minus minima) of the averages of three independent subregions containing the three largest sunspots. Note that the vertical scale differs from those in the figures for the umbrae and penumbrae.

$\delta\tau_{\text{diff}}$  varies from slightly negative at low frequencies to slightly positive at high frequencies and is mostly independent of phase speed.

It is noteworthy that essentially all of the travel-time shifts observed in Figures 5–7 show significant frequency variations. At smaller phase speeds, the variations of both mean travel-time shifts and travel-time asymmetries show strong variations, which often include a change of sign of the shifts. At higher phase speeds, the mean travel-time shifts also show large systematic frequency variations. The mean shifts observed at 5 mHz, for example, are typically twice the value at 3 mHz, with the difference being about 15–20 seconds.

The effects of dispersion, including changes of ray paths as a function of temporal frequency (*e.g.*, Barnes and Cally, 2001), may cause frequency variations of travel-time shifts. However, the frequency variations in the mean travel-time shifts observed here may be much larger than are expected for sound-speed perturbations inferred from recent inversions of travel times. Using the ray approximation, Braun and Birch (2006) computed differences of the mean travel-time shifts between 3 and 5 mHz, for a sound-speed perturbation similar to that of Kosovichev, Duvall, and Scherrer (2000), of about five to ten seconds for phase speeds less than  $30 \text{ km s}^{-1}$ , and less than one to two seconds for higher phase speeds. The implications of these variations are best explored in the context of modeling (and some initial efforts are addressed in Paper 2). However, it is expected that observations such as shown in Figures 5–7 may lead to methods for identifying and removing surface effects. There are no precedents in either global or local helioseismic inversions that offer any hope of including the contribution of unresolved near-surface structure without making use of the temporal frequency dependencies of the observables.

### 3.2. Ridge Filters

In this section, we present results obtained by using filters that isolate individual  $p$ -mode ridges. The use of ridge filters allows us to judge the sensitivity of the travel-time shifts (especially those experienced by waves near the  $p_1$  ridge) to the choice of filter. Ridge-based filters also facilitate a more direct comparison with results obtained with Fourier–Hankel decomposition (see Section 3.3). Ridge filters have been used previously in time–distance helioseismology for  $f$ -mode studies (e.g., Duvall and Gizon, 2000; Gizon and Birch, 2002; Jackiewicz *et al.*, 2007a, 2007b), and recently for  $p$  modes (Jackiewicz, Gizon, and Birch, 2008). Here we employ filters for HH that isolate the  $p_1$ ,  $p_2$ ,  $p_3$ , and  $p_4$  ridges. At each temporal frequency, the filters have full transmission for wavenumbers spanning the midpoints between the desired ridge and the neighboring ridges. Sharp Gaussian roll-offs (similar to those used to remove the  $f$  mode in combination with the phase-speed filters in Section 3.1) remove the contributions above and below these wavenumbers.

Unlike the common use of ray theory to define the radii of annuli (TD) or pupils (HH), there is no “standard” procedure for adopting a pupil geometry for ridge filters. After some trial and error, we settled on a fixed pupil for each ridge. We found that the results were not largely dependent on the outer pupil radius, but they did change significantly with the choice of inner pupil radius. A choice of inner pupil radius smaller than roughly the horizontal  $p$ -mode wavelength of the highest wavenumber present in the power spectra apparently produces undesired leakage of the oscillatory signal at the focus directly into the egression and ingression regressions. With these considerations, we adopted a set of pupils with radii 9–42 Mm ( $p_1$ ), 12–90 Mm ( $p_2$ ), 14–167 Mm ( $p_3$ ), and 17–195 Mm ( $p_4$ ). We have also experimented with varying the width of the frequency bandpass. The travel-time shift maps analyzed here were made with  $\Delta\nu = 0.26$  mHz and were critically sampled with a frequency spacing of  $\Delta\nu/2$ .

The results for the mean travel-time shifts, averaged over umbrae, penumbrae, and plage, are shown in Figure 8, whereas the results for the travel-time differences are shown in Figure 9. In light of the results obtained by using phase-speed filters (Section 3.1), what is most striking from Figures 8 and 9 is that both the mean and difference travel-time shifts obtained by using ridge filters are essentially (with a few noisy exceptions) always negative. This is also true along the  $p_1$  ridge. Comparisons between the ridge-filtered and phase-filtered results are facilitated by overlaying the nearest phase-speed-determined values on Figures 8 and 9. By “nearest” we mean that for a given 1-mHz-frequency bandpass and radial order, the nearest phase-speed filter is that closest to the phase speed of the ridge at the central frequency. For  $p_1$ , the nearest filter combinations are 2F, 3C, 4B, and 5B. For  $p_2$ , these combinations are 2J, 3E, 4D, and 5C. For  $p_3$ , they are 3I, 4E, and 5D, and for  $p_4$ , they are 4H and 5E. For  $p_2$ ,  $p_3$ , and  $p_4$  there is very good agreement between phase-speed and ridge-filtered results for the mean travel-time shifts averaged in umbrae or penumbrae, and reasonable agreement for the time differences. The largest discrepancies are clearly in the  $p_1$  ridge and (especially in the umbrae) involve a change in sign in the measurements of  $\tau_{\text{mean}}$  and  $\tau_{\text{diff}}$  between the two types of filters.

It is noteworthy that the discrepancies between ridge-filtered and phase-speed-filtered results are largest for phase-speed filters with frequency bandwidths that are centered below  $p_1$ . These are the same phase-speed and frequency combinations that produce the positive travel-time shifts seen in Figures 1 and 2. In contrast, adjacent phase-speed filters centered above the  $p_1$  ridge apparently produce travel-time shifts in sunspot umbrae and penumbrae (*i.e.*, the black and magenta squares in the top panels of Figures 8 and 9), which are very close to that observed with the  $p_1$  ridge filter. Repeating the ridge-filtered measurements for some of the cases where these sign changes occur (e.g., near filter 3C) with the

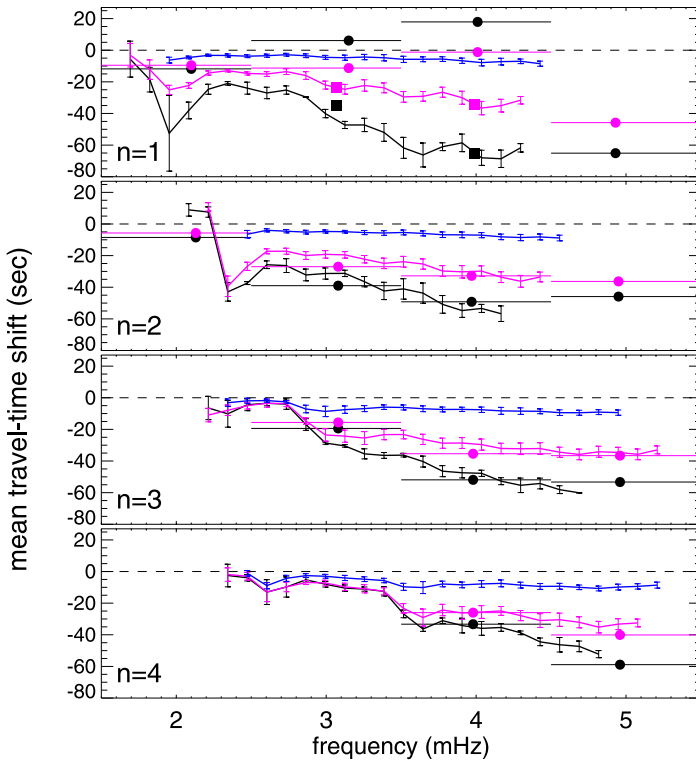


**Figure 8** Mean travel-time shifts determined by using ridge filters and averaged over umbrae (black lines), penumbrae (magenta lines), and plage (blue lines), as functions of frequency along the  $p_1 - p_4$  ridges. Vertical bars indicate the total deviation (maxima minus minima) of the averages of three independent subregions containing the three largest sunspots. The filled black and magenta circles (with 1-mHz-wide horizontal bars) represent comparisons of umbral and penumbral time shifts determined from travel-time maps made with “nearby” phase-speed filters (see text). The circles are placed at the power-weighted average frequency for the given filter and frequency combination. The squares shown near 3 and 4 mHz in the top panel indicate umbral (black) and penumbral (magenta) mean travel-time shifts for the phase-speed filters (3D and 4C), which have higher values of phase speed compared to those denoted by the filled circles (3C and 4B).

same pupil as used with the phase-speed filter yields deviations in both the mean shifts and travel-time asymmetry of only a few seconds (out of a total of 30–40 seconds) from results obtained by using the fixed pupil range stated earlier. Thus, the discrepancy in the sign of travel-time perturbations between the two types of filters is not the result of using different pupils.

Figure 10 illustrates the extreme sensitivity of the sign of the travel-time shifts in sunspots near the  $p_1$  ridge on the choice of filters. This figure compares the results of travel-time shifts computed with a commonly used TD phase-speed filter (filter 1 of Couvidat, Birch, and Kosovichev, 2006, and Zhao and Kosovichev, 2006; hereafter TD1) with shifts computed with a  $p_1$  ridge filter over a frequency bandpass between 3.5 and 5.5 mHz. Despite the gross similarity of the filtered power included in the measurements, the resulting maps of  $\tau_{\text{mean}}$  and  $\tau_{\text{diff}}$  are drastically different. The travel-time shift maps made with the TD1 filter have larger positive values (e.g., by about a factor of two in the mean travel-time shift and a factor of four in the travel-time asymmetry in the penumbrae) than results obtained

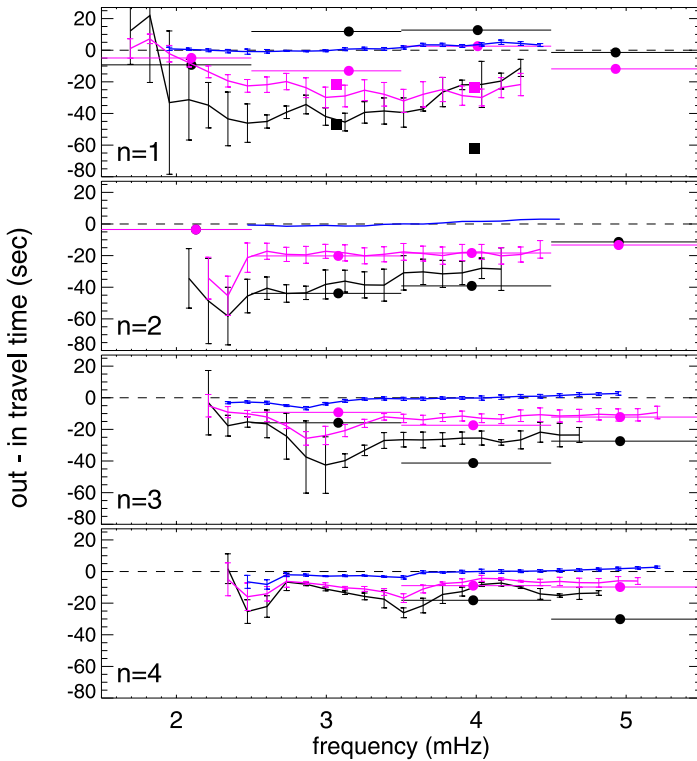


**Figure 9** Difference travel-time shifts determined by using ridge filters in the same format as Figure 8.

with the filter 5A shown in Figure 1, even though the mean phase speed of these filters are both approximately  $13 \text{ km s}^{-1}$ . We have found that incrementally increasing the width of a phase-speed filter, centered at  $12.8 \text{ km s}^{-1}$ , produces maps with incrementally stronger positive travel-time shifts in sunspots. Based on our experience with a variety of filters, we find in general that the requirement for producing positive travel-time shifts appears to be a disproportionate contribution to the correlations of wave power from the low-frequency wing of the  $p_1$  ridge relative to the high-frequency wing. This is illustrated in Figure 11. This asymmetry apparently results from the fact that the mean phase speed of the filter ( $12.8 \text{ km s}^{-1}$ ; shown by the dashed line in Figure 10a) falls significantly below the  $p_1$  ridge.

The reasons for the strong sensitivity, including sign changes, of the travel-time shifts to details of the filter (*e.g.*, width) and the relative weighting of the low-frequency wing of  $p_1$  are not fully understood at this time. Thompson and Zharkov (2008) have presented evidence that a sign switch in mean travel-time shifts also apparently occurs with the application of filters centered half-way (*i.e.*, in the trough) between the  $p_1$  and  $p_2$  ridges.

### 3.3. Comparison with Fourier–Hankel Analysis

Here we compare the ridge-filtered (mean) travel-time shifts with the phase shifts observed in sunspots obtained by using Fourier–Hankel (FH) analysis (Braun, 1995). To do this, we use the published values of phase shifts determined from FH decomposition of waves around two sunspot groups, NOAA 5229 and 5254, observed with Ca II intensity images made at

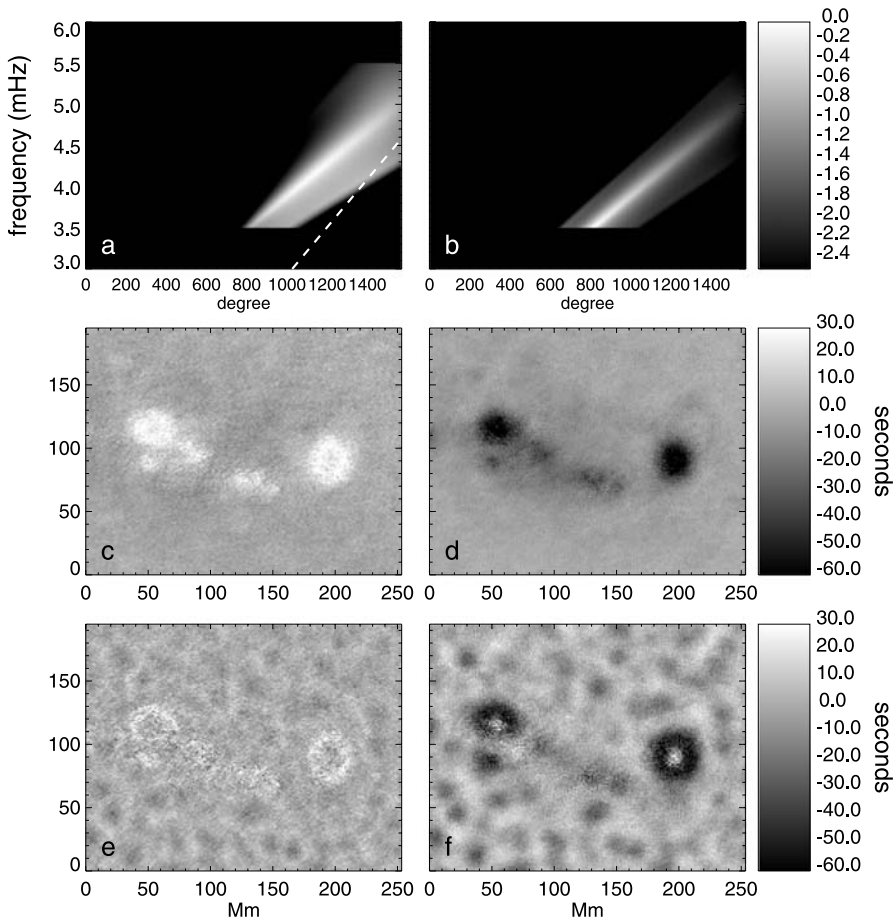


**Figure 10** (a) Azimuthally averaged MDI power spectrum multiplied by phase-speed filter “1” of Couvidat, Birch, and Kosovichev (2006). The gray scale indicates the logarithm of the power, normalized to the peak power. The dashed line indicates the mean phase speed of the filter ( $w = 12.8 \text{ km s}^{-1}$ ). (b) The power spectrum at frequencies between 3.5 and 5.5 mHz multiplied by a  $p_1$  ridge filter, normalized to the peak power. (c) Mean travel-time shifts determined by using the phase-speed filter. (d) Mean shifts determined by using the ridge filter. (e) Travel-time differences determined by using the phase-speed filter. (f) Travel-time differences determined by using the ridge filter.

the geographic South Pole (Braun, 1995). Fortunately, the sunspots studied by Braun (1995) are similar in size to those included in this work. As noted in an earlier comparison with TD measurements (Braun, 1997), the phase shifts in FH analysis are divided by twice the angular frequency for comparison with travel-time shifts (with a switch in the sign of the Hankel results also being needed owing to different Fourier transform conventions). The results are shown in Figure 12. The agreement between the two sets of measurements is very respectable, despite differences in methods and data sets. In particular, the agreement is significantly better than an earlier comparison between FH phase shifts and TD travel-time shifts of Braun (1997), which may be due to the poorer spatial resolution and lack of mode discrimination (*i.e.*, lack of filtering) in that study. The agreement is especially good for the  $p_3$  and  $p_4$  ridges, and it is fair for the  $p_2$  ridge. There are clear, systematic differences for

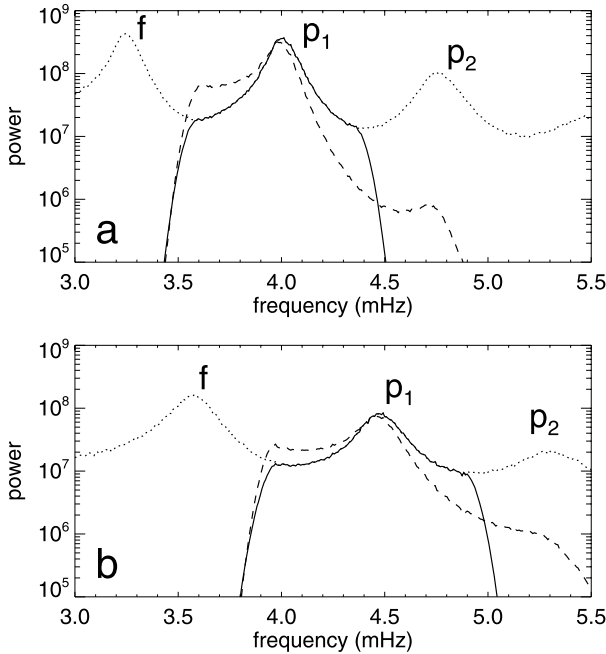


**Figure 11** Cuts of the power as a function of frequency at two fixed wavenumbers illustrating the effect of the filters shown in Figure 10. (a) Power at a constant spatial wavenumber corresponding to a spherical harmonic degree of 1055. The dotted line indicates the unfiltered power, with the  $f$ ,  $p_1$ , and  $p_2$  ridges labeled. The solid line shows the power multiplied by the ridge filter for  $p_1$ . The dashed line indicates the power multiplied by a commonly used time – distance phase speed filter (TD1; see text). For comparison with the ridge-filtered power spectra, the phase-speed-filtered power spectrum is multiplied by a factor so that the integrated power over the frequency bandwidth is the same as the ridge-filtered spectrum. (b) Power as wavenumber corresponding to a spherical harmonic degree of 1230. For both cases, it is clear that the principle difference between the two filter types is the relative weighting of the two wings of the  $p_1$  ridge, such that the phase-speed filter enhances the contribution of the low-frequency wing relative to the high-frequency wing.

$p_1$ , however, with the FH results, indicating stronger travel-time shifts at higher frequencies than the HH results.

Even under ideal circumstances, the two methods (FH decomposition and surface-focused HH) may be expected to yield systematic differences. For example, surface-focused HH (like TD) is primarily sensitive to the set of wave components that propagate to the surface at chosen locations, unlike FH decomposition, which provides no such discrimination. At low phase speeds, for example, phase shifts and absorption coefficients determined from FH analysis include contributions from wave components passing under the sunspot, and at high phase speeds include contributions from waves that refract to the surface multiple times in the sampling annulus. The expectation is that the results of FH analysis may be less sensitive to perturbations at the target than those obtained by using TD or HH. In light of these considerations, the agreement shown in Figure 12 is remarkable.

Maps of the ratio of egression to ingress ion power ( $|H_+|^2/|H_-|^2$ ) can be used in surface-focused HH to probe local emission and absorption properties. Representative maps of this quantity, computed from several frequency bandpasses by using the  $p_1$  (top panels) and  $p_3$  (bottom panels) ridge filters, are shown in Figure 13. The quantity  $\alpha_{HH} = 1 - |H_+|^2/|H_-|^2$  (which we denote as the HH absorption parameter) can be directly compared with the

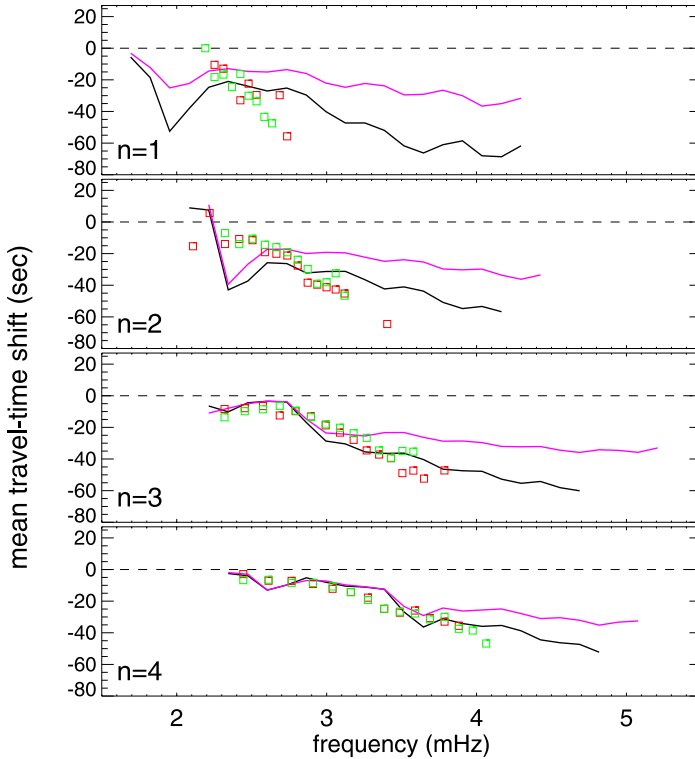


**Figure 12** The mean travel-time shift determined by using ridge filters and averaged over umbrae (black lines) and penumbrae (magenta lines) as shown in Figure 8 as a function of frequency along the  $p_1 - p_4$  ridges. The squares represent equivalent travel-time shifts determined by previously published FH decomposition methods applied to two sunspots, NOAA 5229 (red) and 5254 (green).

absorption coefficients determined by using FH decomposition measurements,  $\alpha_{\text{FH}}$  (Figure 14). The FH absorption coefficients are typically smaller than the surface-focused HH absorption parameter in either the umbrae or penumbrae. Peak values of  $\alpha_{\text{HH}}$  of around 0.7 are observed in sunspot umbrae as compared to typical peak values of  $\alpha_{\text{FH}}$  of around 0.5. Also striking is the difference in behavior of  $\alpha_{\text{FH}}$  and  $\alpha_{\text{HH}}$  at high frequencies, with the absorption parameter from FH methods decreasing toward zero at much lower frequencies than the absorption parameter determined from HH. Some prior HH measurements have shown evidence for this behavior (Lindsey and Braun, 1999), and it has been speculated that the presence of surrounding emission (called “acoustic glories”), which may not be readily resolved by FH decomposition methods, may be at least partly responsible for the lower observed values of  $\alpha_{\text{FH}}$ . It is highly likely that the high-frequency (*e.g.*,  $\nu \geq 5$  mHz) properties of the measured absorption parameters are determined not only by actual absorption mechanisms in the sunspots but by local emission properties as well. For example, a decrease in the local emission can in principle decrease the egression power, and hence the HH absorption parameter. What is known from measurements of  $p$ -mode lifetimes suggests that such a mechanism, as an explanation for all apparent absorption, is not viable for waves at lower frequencies, where the contribution of acoustic flux actually originating at a given target is expected to be only a very small fraction of the total observed egression (or outgoing) power

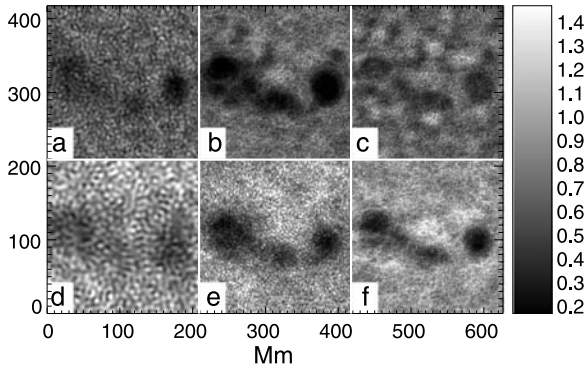
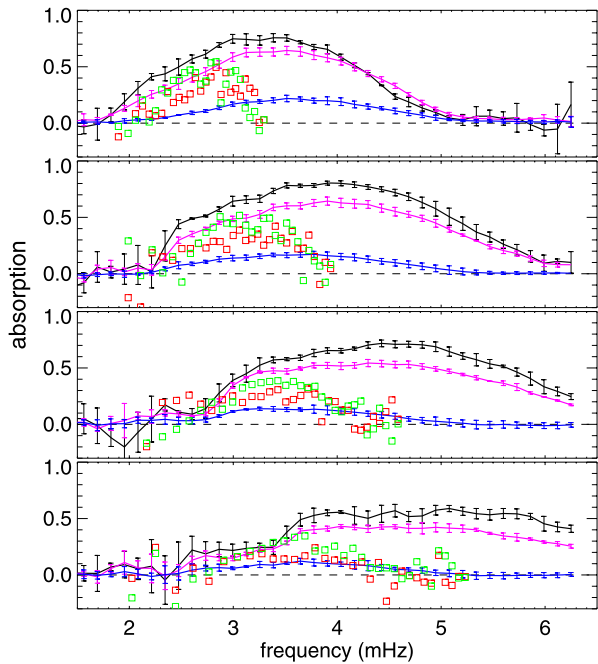


**Figure 13** Maps of the ratio of egression to ingression power determined by using ridge filters and 0.26-mHz-wide frequency bandpasses centered at (a) 2.47 mHz, (b) 3.52 mHz, and (c) 4.55 mHz along the  $p_1$  ridge and (d) 2.99 mHz, (e) 4.04 mHz, and (f) 5.08 mHz along the  $p_3$  ridge. At all frequencies, the areas containing sunspots (and other magnetic flux) are dark, which corresponds to  $\alpha_{HH} > 1$ . At high frequencies (panels c and f), however, note the additional presence of brighter regions.

**Figure 14** The surface-focus HH absorption parameter  $\alpha_{HH}$  determined by using ridge filters and averaged over umbrae (black lines) and penumbrae (magenta lines) as shown in Figure 8 and plage (blue lines) as a function of frequency along the  $p_1 - p_4$  ridges. The squares represent values of the absorption coefficient determined by previously published Fourier–Hankel decomposition methods  $\alpha_{FH}$  applied to two sunspots, NOAA 5229 (red) and 5254 (green).



(Braun, Duvall, and LaBonte, 1987). Finally, we urge caution regarding any interpretation of the observed fall-off of  $\alpha_{HH}$  shown in Figure 14. No attempt has been made to assess (and remove) any “background” contributions to the measured egression and ingression (*e.g.*, contributions from locally generated oscillatory motion occurring within the pupils over which the ingression and egression amplitudes are evaluated). Thus, the observed decrease toward zero of the HH absorption measurements may be unphysical.

## 4. Discussion

It is our preference to let most of the results, as presented through Figures 1 – 14, speak for themselves. A summary of these observations would likely be either too lengthy or otherwise incomplete in that potentially important relationships not directly addressed the text may be neglected. It ought to be fairly clear from observations such as these, however, that the interaction between solar magnetic regions and acoustic waves is highly complex and that no existing model is sufficient in explaining or predicting the complete range of observed behavior. In addition, it should be kept in mind that our observations represent measurements of only three active regions, with only one observable, using one spectral line, and along (essentially) one line-of-sight. It is known, from other observations, that dependencies of phase or travel-times shifts on these and other variables are now recognized, if not fully understood. Deep-focus methods (as applied to TD or HH analyses) are expected to provide further important constraints on models. We also note that we have only briefly touched on the observations relevant to  $p$ -mode absorption in magnetic fields, with the expectation that we will return to this in further publications.

An open question is the degree to which “surface effects” – unknown or unaccounted for physical influences of magnetic fields on acoustic waves – are important in the modeling of subsurface structure of sunspots and active regions. As the set of observations shown here confirms and expands upon those presented by Braun and Birch (2006), it is worth restating the general conclusions derived there. Namely, the strong frequency variation of the measured travel-time shifts cannot be explained by using standard assumptions (*i.e.*, standard ray-approximation-based modeling applied to sound-speed models that are typical of published 3D inversion results). To these unexplained frequency variations must now be added apparently “anomalous” positive travel-time shifts (both the mean and travel-time asymmetry) in sunspots, so called here because the conditions (*i.e.*,  $p$ -mode properties and choice of filter) under which they appear defy the expectations of standard assumptions and models. We will return to both of these issues, in the context of models of sound-speed perturbations, in Paper 2.

It has been argued (*e.g.*, Zhao and Kosovichev, 2006) that the sign change of travel-time shifts with varying phase speed provides evidence for the relative lack of importance of surface effects for standard inferences from 3D inversions. Certainly, a change of sign is not a typical property of known “surface terms” in models of frequency shifts in structural inversions in global helioseismology and ring-diagram analyses. However, rather than identify the sensitivity of the sign of  $\tau_{\text{mean}}$  or  $\tau_{\text{diff}}$  to the choice of filter with a magnetic surface effect, these observations seriously raise the possibility that the positive values of these shifts represent an artifact, by which we mean a property that is more sensitive to the methods of the analysis than to actual physical conditions within or below sunspots.

**Acknowledgements** We thank an anonymous referee for useful suggestions. This work is supported by funding through NASA Contract Nos. NNH04CC05C, NNH05CC76C, and NNG07E151C, NSF Grant No. AST-0406225, and a subcontract through the HMI project at Stanford University awarded to NWRA.

## References

- Barnes, G., Cally, P.S.: 2001, Frequency dependent ray paths in local helioseismology. *Publ. Astron. Soc. Aust.* **18**, 243–251.
- Basu, S., Antia, H.M., Bogart, R.S.: 2004, Ring-diagram analysis of the structure of solar active regions. *Astrophys. J.* **610**, 1157–1168.

- Benson, D., Stein, R., Nordlund, Å.: 2006, Supergranulation scale convection simulations. In: Uitenbroek, H., Leibacher, J., Stein, R.F. (eds.) *Solar MHD Theory and Observations: A High Spatial Resolution Perspective*, *Astron. Soc. Pac. Conf. Ser.* **354**, Astron. Soc. Pac., San Francisco, 92–96.
- Birch, A.C., Braun, D.C., Hanasoge, S.M.: 2008, Surface-focused seismic holography of sunspots: II. Expectations from numerical simulations using sound-speed perturbations. *Solar Phys.*, submitted (Paper 2).
- Bogdan, T.J.: 2000, Sunspot oscillations: A review. *Solar Phys.* **192**, 373–394.
- Bogdan, T.J., Braun, D.C.: 1995, Active region seismology. In: Hoeksema, J.T., Domingo, V., Fleck, B., Battrick, B. (eds.) *Helioseismology*, *SP-376*, ESA, Noordwijk, 31–45.
- Bogdan, T.J., Brown, T.M., Lites, B.W., Thomas, J.H.: 1993, The absorption of  $p$  modes by sunspots – variations with degree and order. *Astrophys. J.* **406**, 723–734.
- Braun, D.C.: 1995, Scattering of  $p$  modes by sunspots. I. Observations. *Astrophys. J.* **451**, 859–876.
- Braun, D.C.: 1997, Time – distance sunspot seismology with GONG data. *Astrophys. J.* **487**, 447–456.
- Braun, D.C., Birch, A.C.: 2006, Observed frequency variations of solar  $p$ -mode travel times as evidence for surface effects in sunspot seismology. *Astrophys. J.* **647**, L187–L190.
- Braun, D.C., Lindsey, C.: 2000, Phase-sensitive holography of solar activity. *Solar Phys.* **192**, 307–319.
- Braun, D.C., Birch, A.C., Lindsey, C.: 2004, Local helioseismology of near-surface flows. In: Danesy, D. (ed.) *SOHO 14 Helio- and Asteroseismology: Towards a Golden Future*, *SP-559*, ESA, Noordwijk, 337–340.
- Braun, D.C., Duvall, T.L. Jr., LaBonte, B.J.: 1987, Acoustic absorption by sunspots. *Astrophys. J.* **319**, L27–L31.
- Braun, D.C., Duvall, T.L. Jr., LaBonte, B.J.: 1988, The absorption of high-degree  $p$ -mode oscillations in and around sunspots. *Astrophys. J.* **335**, 1015–1025.
- Braun, D.C., Duvall, T.L. Jr., Labonte, B.J., Jefferies, S.M., Harvey, J.W., Pomerantz, M.A.: 1992, Scattering of  $p$  modes by a sunspot. *Astrophys. J.* **391**, L113–L116.
- Cally, P.S., Crouch, A.D., Braun, D.C.: 2003, Probing sunspot magnetic fields with  $p$ -mode absorption and phase shift data. *Mon. Not. Roy. Astron. Soc.* **346**, 381–389.
- Cameron, R., Gizon, L., Daifallah, K.: 2007, SLiM: A code for the simulation of wave propagation through an inhomogeneous, magnetised solar atmosphere. *Astron. Nachr.* **328**, 313–318.
- Cameron, R., Gizon, L., Duvall, T. Jr.: 2008, Helioseismology of sunspots: Confronting observations with three-dimensional MHD simulations of wave propagation. *Solar Phys.*, submitted.
- Chou, D.Y.: 2000, Acoustic imaging of solar active regions. *Solar Phys.* **192**, 241–259.
- Christensen-Dalsgaard, J., Gough, D.O., Perez Hernandez, F.: 1988, Stellar disharmony. *Mon. Not. Roy. Astron. Soc.* **235**, 875–880.
- Couvidat, S., Rajaguru, S.P.: 2007, Contamination by surface effects of time – distance helioseismic inversions for sound speed beneath sunspots. *Astrophys. J.* **661**, 558–567.
- Couvidat, S., Birch, A.C., Kosovichev, A.G.: 2006, Three-dimensional inversion of sound speed below a sunspot in the Born approximation. *Astrophys. J.* **640**, 516–524.
- Couvidat, S., Birch, A.C., Kosovichev, A.G., Zhao, J.: 2004, Three-dimensional inversion of time – distance helioseismology data: Ray-path and Fresnel-zone approximations. *Astrophys. J.* **607**, 554–563.
- Crouch, A.D., Cally, P.S., Charbonneau, P., Braun, D.C., Desjardins, M.: 2005, Genetic magnetohelioseismology with Hankel analysis data. *Mon. Not. Roy. Astron. Soc.* **363**, 1188–1204.
- Duvall, T.L. Jr., Gizon, L.: 2000, Time – distance helioseismology with  $f$  modes as a method for measurement of near-surface flows. *Solar Phys.* **192**, 177–191.
- Duvall, T.L. Jr., D’Silva, S., Jefferies, S.M., Harvey, J.W., Schou, J.: 1996, Downflows under sunspots detected by helioseismic tomography. *Nature* **379**, 235–237.
- Fan, Y., Braun, D.C., Chou, D.Y.: 1995, Scattering of  $p$  modes by sunspots. II. Calculations of phase shifts from a phenomenological model. *Astrophys. J.* **451**, 877–888.
- Giles, P.M.: 2000, Time – distance measurements of large-scale flows in the solar convection zone. Ph.D. thesis, Stanford University.
- Gizon, L., Birch, A.C.: 2002, Time – distance helioseismology: The forward problem for random distributed sources. *Astrophys. J.* **571**, 966–986.
- Gizon, L., Birch, A.C.: 2005, Local helioseismology. *Liv. Rev. Solar Phys.* **2**. <http://www.livingreviews.org/lrsp-2005-6> (cited on 14 February 2008).
- Gizon, L., Duvall, T.L. Jr., Larsen, R.M.: 2000, Seismic tomography of the near solar surface. *J. Astrophys. Astron.* **21**, 339–342.
- Gordovskyy, M., Jain, R.: 2007, Scattering of  $p$  modes by a thin magnetic flux tube. *Astrophys. J.* **661**, 586–592.
- Hanasoge, S.M., Duvall, T.L. Jr.: 2007, The solar acoustic simulator: Applications and results. *Astron. Nachr.* **328**, 319–322.
- Hanasoge, S.M., Duvall, T.L. Jr., Couvidat, S.: 2007, Validation of helioseismology through forward modeling: Realization noise subtraction and kernels. *Astrophys. J.* **664**, 1234–1243.

- Hanasoge, S.M., Couvidat, S., Rajaguru, S.P., Birch, A.C.: 2007, Impact of locally suppressed wave sources on helioseismic travel times. *Astrophys. J.*, submitted. <http://arxiv.org/abs/0707.1369v3>.
- Hughes, S.J., Rajaguru, S.P., Thompson, M.J.: 2005, Comparison of GONG and MDI: Sound-speed anomalies beneath two active regions. *Astrophys. J.* **627**, 1040–1048.
- Jackiewicz, J., Gizon, L., Birch, A.C.: 2008, High-resolution mapping of flows in the solar interior: Fully consistent OLA inversion of helioseismic travel times. *Solar Phys.*, submitted.
- Jackiewicz, J., Gizon, L., Birch, A.C., Duvall, T.L. Jr.: 2007a, Time-distance helioseismology: Sensitivity of  $f$ -mode travel times to flows. *Astrophys. J.* **671**, 1051–1064.
- Jackiewicz, J., Gizon, L., Birch, A.C., Thompson, M.J.: 2007b, A procedure for the inversion of  $f$ -mode travel times for solar flows. *Astron. Nachr.* **328**, 234–239.
- Jensen, J.M., Duvall, T.L. Jr., Jacobsen, B.H.: 2003, Noise propagation in inversion of helioseismic time–distance data. In: Sawaya-Lacoste, H. (ed.) *GONG+ 2002. Local and Global Helioseismology: The Present and Future*, SP-517, ESA, Noordwijk, 315–318.
- Jensen, J.M., Duvall, T.L. Jr., Jacobsen, B.H., Christensen-Dalsgaard, J.: 2001, Imaging an emerging active region with helioseismic tomography. *Astrophys. J.* **553**, L193–L196.
- Khomenko, E., Collados, M.: 2006, Numerical modeling of magnetohydrodynamic wave propagation and refraction in sunspots. *Astrophys. J.* **653**, 739–755.
- Korzennik, S.G.: 2006, The cookie cutter test for time–distance tomography of active regions. In: *Proceedings of SOHO 18/GONG 2006/HELAS I, Beyond the Spherical Sun*, SP-624, ESA, Noordwijk, 60.
- Kosovichev, A.G.: 1996, Tomographic imaging of the Sun's interior. *Astrophys. J.* **461**, L55–L57.
- Kosovichev, A.G., Duvall, T.L. Jr.: 1997, Acoustic tomography of solar convective flows and structures. In: Pijpers, F.P., Christensen-Dalsgaard, J., Rosenthal, C.S. (eds.) *SCORE '96: Solar Convection and Oscillations and their Relationship*, *Astrophys. Spa. Science* **225**, 241–260.
- Kosovichev, A.G., Duvall, T.L. Jr., Scherrer, P.H.: 2000, Time–distance inversion methods and results. *Solar Phys.* **192**, 159–176.
- Lindsey, C., Braun, D.C.: 1997, Helioseismic holography. *Astrophys. J.* **485**, 895–903.
- Lindsey, C., Braun, D.C.: 1999, Chromatic holography of the sunspot acoustic environment. *Astrophys. J.* **510**, 494–504.
- Lindsey, C., Braun, D.C.: 2000, Basic principles of solar acoustic holography. *Solar Phys.* **192**, 261–284.
- Lindsey, C., Braun, D.C.: 2004a, Principles of seismic holography for diagnostics of the shallow subphotosphere. *Astrophys. J. Suppl.* **155**, 209–225.
- Lindsey, C., Braun, D.C.: 2004b, The penumbral acoustic anomaly. In: Danesy, D. (ed.) *SOHO 14 Helio- and Asteroseismology: Towards a Golden Future*, SP-559, ESA, Noordwijk, 552.
- Lindsey, C., Braun, D.C.: 2005a, The acoustic showerglass. I. Seismic diagnostics of photospheric magnetic fields. *Astrophys. J.* **620**, 1107–1117.
- Lindsey, C., Braun, D.C.: 2005b, The acoustic showerglass. II. Imaging active region subphotospheres. *Astrophys. J.* **620**, 1118–1131.
- Lindsey, C., Schunker, H., Cally, P.S.: 2007, Magnetoseismic signatures and flow diagnostics beneath magnetic regions. *Astron. Nachr.* **328**, 298–304.
- Lites, B.W.: 1992, Sunspot oscillations—observations and implications. In: Thomas, J.H., Weiss, N.O. (eds.) *NATO ASIC Proc. 375: Sunspots. Theory and Observations*, Kluwer, Dordrecht, 261–302.
- Mansour, N.N., Kosovichev, A.G., Georgobiani, D., Wray, A., Miesch, M.: 2004, Turbulence convection and oscillations in the Sun. In: Danesy, D. (ed.) *SOHO 14 Helio- and Asteroseismology: Towards a Golden Future*, SP-559, ESA, Noordwijk, 164–171.
- Parchevsky, K.V., Zhao, J., Kosovichev, A.G.: 2008, Influence of non-uniform distribution of acoustic wave-field strength on time–distance helioseismology measurements. *Astrophys. J.*, submitted.
- Rajaguru, S.P., Birch, A.C., Duvall, T.L. Jr., Thompson, M.J., Zhao, J.: 2006, Sensitivity of time–distance helioseismic measurements to spatial variation of oscillation amplitudes. I. Observations and a numerical model. *Astrophys. J.* **646**, 543–552.
- Rajaguru, S.P., Sankarasubramanian, K., Wachter, R., Scherrer, P.H.: 2007, Radiative transfer effects on Doppler measurements as sources of surface effects in sunspot seismology. *Astrophys. J.* **654**, L175–L178.
- Scherrer, P.H., Bogart, R.S., Bush, R.I., Hoeksema, J.T., Kosovichev, A.G., Schou, J., Rosenberg, W., Springer, L., Tarbell, T.D., Title, A., Wolfson, C.J., Zayer, I., MDI Engineering Team: 1995, The solar oscillations investigation—Michelson Doppler imager. *Solar Phys.* **162**, 129–188.
- Schunker, H., Cally, P.S.: 2006, Magnetic field inclination and atmospheric oscillations above solar active regions. *Mon. Not. Roy. Astron. Soc.* **372**, 551–564.
- Schunker, H., Braun, D.C., Cally, P.S.: 2007, Surface magnetic field effects in local helioseismology. *Astron. Nachr.* **328**, 292–297.
- Schunker, H., Braun, D.C., Cally, P.S., Lindsey, C.: 2005, The local helioseismology of inclined magnetic fields and the showerglass effect. *Astrophys. J.* **621**, L149–L152.

- Shelyag, S., Erdélyi, R., Thompson, M.J.: 2006, Forward modeling of acoustic wave propagation in the quiet solar subphotosphere. *Astrophys. J.* **651**, 576–583.
- Shelyag, S., Erdélyi, R., Thompson, M.J.: 2007, Forward modelling of sub-photospheric flows for time–distance helioseismology. *Astron. Astrophys.* **469**, 1101–1107.
- Simmons, B., Basu, S.: 2003, A method for inverting high-degree modes. In: Sawaya-Lacoste, H. (ed.) *GONG+ 2002. Local and Global Helioseismology: The Present and Future*, SP-517, ESA, Noordwijk, 393–396.
- Thomas, J.H., Cram, L.E., Nye, A.H.: 1982, Five-minute oscillations as a subsurface probe of sunspot structure. *Nature* **297**, 485–487.
- Thompson, M.J., Zharkov, S.: 2008, Recent developments in local helioseismology. *Solar Phys.* doi:[10.1007/s11207-008-9143-6](https://doi.org/10.1007/s11207-008-9143-6).
- Tong, C.H., Thompson, M.J., Warner, M.R., Pain, C.C.: 2003, Helioseismic signals and wave field helioseismology. *Astrophys. J.* **593**, 1242–1248.
- Werne, J., Birch, A., Julien, K.: 2004, The need for control experiments in local helioseismology. In: Danesy, D. (ed.) *SOHO 14 Helio- and Asteroseismology: Towards a Golden Future*, SP-559, ESA, Noordwijk, 172–181.
- Woodard, M.F.: 1997, Implications of localized, acoustic absorption for heliotomographic analysis of sunspots. *Astrophys. J.* **485**, 890–894.
- Zhao, J., Kosovichev, A.G.: 2003, Helioseismic observation of the structure and dynamics of a rotating sunspot beneath the solar surface. *Astrophys. J.* **591**, 446–453.
- Zhao, J., Kosovichev, A.G.: 2006, Surface magnetism effects in time–distance helioseismology. *Astrophys. J.* **643**, 1317–1324.
- Zhao, J., Kosovichev, A.G., Duvall, T.L. Jr.: 2001, Investigation of mass flows beneath a sunspot by time–distance helioseismology. *Astrophys. J.* **557**, 384–388.